



# AstroComb(v.1.0): Non-linear, Multi-channel, Probabilistic Cyclostratigraphic Analysis

Iris Fernandes<sup>\*1</sup>, Klaus Mosegaard<sup>1</sup>, Aske L. Sørensen<sup>2</sup>, Mohammad  
Youssof<sup>1</sup>, Nicolas Thibault<sup>2</sup>, and Tais W. Dahl<sup>2</sup>

<sup>1</sup>Niels Bohr Institute, University of Copenhagen, Denmark

<sup>2</sup>Department of Geosciences and Natural Resource Management, University  
of Copenhagen, Denmark

## Abstract

We present a new algorithm for constructing floating astronomical timescales with explicit uncertainty estimates from sedimentary sequences. The method integrates probabilistic spectral analysis with inverse geochronological modeling, applied to ultra-high-resolution, multiproxy datasets such as core scanning X-Ray Fluorescence (XRF) elemental records. Our framework does not smooth data or impose layer-to-layer dependency, allowing sedimentation rates to vary abruptly at short stratigraphic length scales. By detecting and statistically constraining Milankovitch cycles preserved in stratigraphic signals, the algorithm seeks a floating age-depth model that can be anchored to astronomical tie points, where available. The resulting timescales enable precise, uncertainty-bounded timing of biostratigraphic zones, geochemical events, and depositional cycles. This approach advances astrochronology by combining cycle detection with formal stratigraphic modelling, while preserving fine-scale depositional variability, offering a reproducible and statistically rigorous framework for dating deep-time records.

## 1 Introduction

Stratigraphic records from sedimentary basins are powerful archives of past environmental variability, recording both long-term geological trends and short-term changes in Earth's climate system. Identifying and decoding these Milankovitch cycles provides an essential tool for reconstructing past timescales — a methodology known as astrochronology.

Traditional astrochronologic approaches typically rely on matching repetitive spectral features in stratigraphic depth-series data to a target set of orbital frequencies, either through spectral filtering (Hays et al. (1976); Weedon (2003); Meyers et al. (2008, 2001)), or tuning

---

\*Corresponding author: iris@nbi.ku.dk



31 against numerical astronomical solutions (TimeOpt: Meyers (2015), TimeOptMCMC: Meyers  
32 and Malinverno (2018); AstroGeoFit: Hoang et al. (2025)) or evolutionary spectral correlation  
33 (eCOCO: Li et al. (2018), eTimeOpt: Meyers (2019)).

34 Despite sedimentation is a punctuated process (Kemp and Sexton (2014)) over shorter  
35 timescales, these cyclostratigraphic methods often assume continuous, smoothly varying sed-  
36 imentation rates or enforce strict stationarity in cycle expression over longer time scales; e.g.  
37 precession period. As a result, current age-depth models likely oversimplify the stratigraphic  
38 record, particularly in cases where sedimentation is punctuated by hiatuses, erosion, rapid  
39 deposition events, authigenic sediment, diagenetic chemical alteration or lithologic transi-  
40 tions. In reality, sediment accumulation in marine basins is controlled by a complex interplay  
41 of sediment supply, accommodation space, bottom water conditions, and diagenesis — all of  
42 which can introduce non-uniformity in the sedimentation rate at fine scales.

43 The continuity-assumption becomes problematic especially over shorter stratigraphic  
44 thickness representing shorter time scales. For example, the approximately 500 million  
45 year-old Cambrian Alum Shale Formation of Scandinavia has been slowly-deposited, and  
46 the shortest Milankovitch periods (19 kyrs) are covered by only 2–12 cm of stratigraphy  
47 (Sørensen et al. (2020); Zhao et al. (2022)). Here, we advocate that spectral matching  
48 to target periodicities must be done probabilistically, and astrochronological models must  
49 accommodate uncertainty in the depositional response to the forcing signal. Fortunately,  
50 these shales consists of finely laminated mud (grain size  $\approx 2 \mu\text{m}$ ) and high-resolution ele-  
51 mental datasets can be obtained at sub-millimeter resolution using Core Scanning X-Ray  
52 Fluorescence (CS-XRF) spectroscopy providing opportunities and challenges for refining as-  
53 trochronological timescales including rigorous error propagation that requires more sophis-  
54 ticated analytical tools.

55 In response to these challenges, we present a probabilistic method to infer instantaneous  
56 sedimentation rates directly from multi-channel geochemical time series data (e.g. elemental  
57 abundances or ratios) by fitting Milankovitch cycles in a locally adaptive manner. Rather  
58 than assuming a constant or globally smoothed rate model, our approach treats sedimenta-  
59 tion as a piecewise continuous process, allowing for abrupt or non-linear changes across the  
60 stratigraphic column. The core innovation is to invert a forward model of spectral signal  
61 generation — simulating how Milankovitch frequencies are expressed across stratigraphic  
62 depth under varying sedimentation rates — to obtain the probability distribution of the  
63 sedimentation rate at each depth, conditioned on observed multi-channel data and a target  
64 astronomical signal.

65 This framework is implemented in a newly developed algorithm, AstroComb, which builds  
66 upon and extends the concepts behind earlier astrochronological tools, such as TimeOptMCMC  
67 (Meyers and Malinverno (2018) and eCOCO Li et al. (2018)), while incorporating uncer-  
68 tainty quantification adapted to high-speed computation on large, multi-channel data sets.  
69 AstroComb applies a windowed, sliding inversion across the stratigraphy, yielding a depth-  
70 resolved series of sedimentation rates and posterior uncertainties. AstroComb allows disconti-  
71 nuities in sedimentation rate where supported by the data — for example, in the presence of  
72 condensed layers, stratigraphic breaks, or sharp facies transitions — which may be essential  
73 for reconstructing realistic depositional histories. Furthermore, AstroComb provides a mea-  
74 sure of the information content of the data at all depths, indicating the uncertainty/reliability  
75 of the sedimentation rate estimates. Importantly, AstroComb calculates the full probability



76 distribution of sedimentation rates based on multi-channel input data, which is essential  
77 input for sub-precession cycle refinement of age-depth relationships using geochemically-  
78 informed sedimentation rates as exercised with ProBE4T (Fernandes et al. (2026)).

79 Here, we apply **AstroComb** to the Fågeltofta-2 core through the later Cambrian Alum  
80 Shale Formation. The core comprises a thick, continuous succession of laminated, organic-  
81 rich, black mudrocks with high pyrite content and strong enrichments in redox sensitive  
82 elements (Dahl et al. (2019)). The Alum shale was deposited extremely slowly ( $\sim 1\text{--}6$  mm/ky,  
83 Nielsen et al. (2018)) on the Baltoscandian passive margin. Using high-resolution XRF data  
84 from over 90,000 measurements across 18 m of stratigraphy at 0.2 mm intervals, previous  
85 cyclostratigraphic analyses have confirmed such slow sedimentation rates (Sørensen et al.  
86 (2020); Zhao et al. (2022)), which we here show are also consistent with **AstroComb** results  
87 presented here. Further, the **AstroComb** results reveal abrupt variation in sedimentation  
88 rates, potentially identifying intervals of slow background accumulation interspersed with  
89 short-duration accumulation events. Potentially, chemical oscillations allow for improved  
90 dating of stratigraphic intervals, duration of event, and lithologic transitions within the core  
91 — with implications for rates of paleoenvironmental change and refinement of the geological  
92 time-scale.

93 **AstroComb** is designed to leverage high-resolution multi-element core data for astrochronol-  
94 ogy in a quantitative probabilistic manner. The algorithm aligns a range of astronomical  
95 periods with recurring signals in the stratigraphy, and extends the capabilities of previous  
96 toolboxes by incorporating multichannel geochemical data and uncertainty quantification  
97 through inverse modeling at each analysis step. Each channel represent elemental abun-  
98 dance (in peak area or concentrations), best fit mineral abundance (in weight percent) or  
99 ratios between XRF peaks areas (e.g. Al/RhCoh, normalized peak area signals).

100 The overarching goal is to detect Milankovitch signals and construct floating astronomical  
101 timescales, while explicitly accounting for uncertainties. The approach is built on four main  
102 components, which constitute the workflow of **AstroComb**:

- 103 • A probabilistic inversion framework to recover, not only the best-fit sedimentation rate  
104 at any given stratigraphic point in an elemental time series, but also uncertainties and  
105 a measure of information content.
- 106 • A generalizable methodology that can be applied to any cyclic geochemical or paleo-  
107 environment signal,
- 108 • A demonstration of how variable sedimentation rates manifest in the spectral expres-  
109 sion of Milankovitch cycles
- 110 • An application to a  $\sim 500$  Ma Cambrian core verifies the preservation of astronomical  
111 signals and evaluate sedimentation rates and their probability distributions (uncer-  
112 tainty) from the information content.

113 By integrating multi-element signal processing, spectral modeling, and inversion theory, our  
114 approach extends the methodological framework of astrochronology into previously unex-  
115 plored domains. It enables the simultaneous analysis of multiple signals and accommodates  
116 probabilistic age-depth models that can be non-smooth, and discontinuous—reflecting the  
117 inherent complexity of real-world sedimentary systems.



## 118 2 Theory and Methods

### 119 2.1 Overview

120 The goal of this study is to reconstruct a *locally varying sedimentation rate profile* from  
121 multiple geochemical depth series, under the assumption that certain stratigraphic signals  
122 (e.g., elemental variability) reflect astronomical forcing. We achieve this by inverting a  
123 forward model of signal distortion under varying sedimentation, using a formulation rooted  
124 in probabilistic inversion.

125 This method builds upon the principles of astrochronology—particularly the spectral  
126 identification of Milankovitch-band periodicities in sedimentary records—but extends them  
127 to allow for *instantaneous, non-stationary sedimentation rates*. **AstroComb** performs a sliding-  
128 window probabilistic fit of observed geochemical spectra to a predefined target astronomical  
129 spectrum, yielding a sedimentation rate that optimally “stretches” or “compresses” the time  
130 axis at each position to recover astronomical frequencies. The fit is performed in frequency  
131 domain, which allows multi-channel (e.g. multiple elements) that will not be obscured if  
132 displaced by a phase-lag.

133 We begin by formalizing the relationship between sedimentation rate and spectral distortion,  
134 then describe the inversion procedure and implementation of **AstroComb**. Finally –  
135 as an example – we discuss its application to the Alum Shale data and compare to previous  
136 results (Sørensen et al. (2020)).

### 137 2.2 Forward Model of Spectral Distortion

138 Let  $d(z)$  be a geochemical depth series (e.g., Al concentrations), where  $z$  is stratigraphic  
139 depth. If sediment accumulated at a locally constant rate  $r(z) = \frac{dz}{dt}$ , then in the time  
140 domain, the corresponding series is  $d(t)$ . However, in practice we only observe the signal in  
141 the depth domain.

142 Let  $k$  be a frequency in the depth domain (wave number in cycles per mm) and  $f$  its  
143 time-domain counterpart (cycles per kyr). The transformation between the two is:

$$k = \frac{f}{r} \quad (1)$$

144 Thus, a fixed astronomical frequency  $f$  will appear in the stratigraphic record as a peak at  
145  $k$ , depending on the local sedimentation rate. Variations in  $r(z)$  distort the signal, shifting,  
146 splitting, or smearing spectral peaks. Our objective is to recover  $r(z)$  such that the observed  
147 power spectrum matches that predicted from astronomical forcing (see Figure 1).

### 148 2.3 Target Astronomical Spectrum

149 Because no closed form orbital solution exists beyond about 50 Ma (Laskar et al. (2011,  
150 2004)), we adopt theoretical periods constructed from studies of deep-time orbital mechanics  
151 (Farhat et al. (2022); Waltham (2015)). For the later Cambrian  $\sim 497$  Ma, the target  
152 includes:

- 153 • Long eccentricity: 405 kyr



- 154 • Short eccentricity: 99 ky
- 155 • Obliquity: 32.4 kyr
- 156 • Precession: 19.5 kyr

157 We encode these as 4 sinusoids with known periods. We do not define their expected  
 158 spectral power ratios based on orbital modulation transfer, since the Earth’s climate and  
 159 environmental response to the Milankovitch forcing modifies these ratios in an unknown  
 160 way.

## 161 2.4 Computing the Likelihood of a Sedimentation Rate

162 For a given depth interval (window) centered at  $z_0$ , we obtain power spectra  $\mathbf{D}_{obs}$  of multiple,  
 163 observed signals ( $\mathbf{D}_{obs}$  is a matrix of spectra with a spectrum of one channel in each column).  
 164 For each trial sedimentation rate  $r$ , we convert the target time-domain frequencies  $f$  to  
 165 expected depth-domain frequencies (wave numbers)  $k = f/r$  and compute *synthetic spectra*

$$\mathbf{G}(r, \mathbf{a}) = \sum_{m=1}^M a_m \mathbf{w} \left( \frac{f_m}{r} \right) \quad (2)$$

166 where  $\mathbf{G}(r, \mathbf{a})$  is a matrix of computed data spectra (a copy of the spectrum in each column),  
 167  $f_m$  is the  $m$ ’th Milankovitch frequency (assumed known), and  $\mathbf{w}(\frac{f_m}{r})$  is the shape of a spectral  
 168 line, centered at  $\frac{f_m}{r}$ . The shape  $\mathbf{w}$  can be computed as the discrete Fourier transform of a  
 169 discretized delta function with the same length as the window.

170 From the synthetic spectra  $\mathbf{G}(r, \mathbf{a})$  and the matrix of observation spectra  $\mathbf{D}_{obs}$  we can  
 171 now calculate the likelihood as the probability of data, given the sedimentation rate  $r$  and  
 172 the spectral peak amplitudes  $\mathbf{a}$ :

$$L(r, \mathbf{a}) = P(\mathbf{D}_{obs} | (r, \mathbf{a})). \quad (3)$$

173 Our computation of the likelihood is done as follows:

- 174 1. As prior information about the data uncertainties, we mimic the ’manual’ process of  
 175 spectral line identification by defining a probability that there is a potential Milankovic  
 176 peak at a given wavenumber  $k$  in the spectrum. Between user-defined lower and upper  
 177 bounds  $a$  (the lower limit for being identified as a ”peak”) and  $b$  (the value above which  
 178 we are sure that we have found a potential peak), the probability increases from a user  
 179 defined, small positive number  $p_a$  at the lower limit to  $p_b = 1 - p_a$  at the upper limit.  
 180 Typical values are  $a = \langle F \rangle + \sigma_F$  and  $b = \langle F \rangle + 3\sigma_F$ , where  $\langle F \rangle$  is a local mean of the  
 181 spectrum around the considered wavenumber  $k$ , and  $\sigma_F$  is the local standard deviation  
 182 of the spectrum. A typical value of the threshold probability  $p_a$  is 0.01. The probability  
 183 is chosen as a smooth, monotonically increasing sigmoid function  $p(x)$  satisfying

$$p(a) = p_a, \quad p_b(b) = 1 - p_a, \quad (4)$$

184 with the constraints

$$b > a, \quad 0 < p_a < 0.5. \quad (5)$$



185 We adopt the logistic sigmoid form

$$p(x) = \frac{1}{1 + \exp(-k(x - x_0))} \quad (6)$$

186 with

$$x_0 = \frac{a + b}{2}. \quad (7)$$

187 2. For each layer (which is  $\Delta z = 0.2$  mm thick in the Fågeltofta-2 core example), we evalu-  
 188 ate the likelihood in a grid of sedimentation rates  $r$  with typical grid spacing  $\Delta r = 0.02$   
 189 mm/ky. Each possible choice corresponds to given locations of the Milankovic cycles  
 190 in the spectrum, and for each location at  $k_i$  with spectral amplitude  $a_i$ , we evaluate  
 191 the probability  $p(k_i, a_i)$ . Finally, the likelihood of the considered sedimentation rate  $\mathbf{r}$   
 192 is computed as the product

$$L(\mathbf{r}) = \prod_{i=1}^{I_M} p(k_i, a_i), \quad (8)$$

193 where  $I_M$  is the number of Milankovic cycles considered. When several records of, e.g.,  
 194 basic elements concentrations are used in the calculation, the combined likelihood for  
 195 all records is computed as the product of the individual likelihoods.

## 196 2.5 The Posterior Probabilities of Sedimentation Rates

197 If prior information about  $(r, \mathbf{a})$  is encoded by a probability density  $\rho(r, \mathbf{a})$  we can - in a  
 198 Bayesian formulation - express the complete, probabilistic solution as a *posterior* probability  
 199 density

$$p(r, \mathbf{a}) = C \cdot L(r, \mathbf{a}) \rho(r, \mathbf{a}). \quad (9)$$

200 where  $C$  is a proportionality constant. In the example below, where data from Fågeltofta-2  
 201 is analyzed, the prior assigns constant values to all sedimentation rates within user-defined  
 202 boundaries of  $1.0 \text{ mm/ky} < r < 10.0 \text{ mm/ky}$ .

203 From the marginal sedimentation rate distribution

$$p(r) = \int p(r, \mathbf{a}) da \quad (10)$$

204 at each stratigraphic position, we can now compute a floating geological time,  $t$ , and its  
 205 uncertainties as a function of depth,  $z$ . If the absolute time,  $t_0$ , is known at a given depth  
 206  $z_0$ , and the sedimentation rate in layer  $n$  is  $r_n$ , the time at  $z_0 + N\Delta z$  is

$$t(z_0 + N\Delta z) = t_0 + \Delta z \sum_{n=1}^N \frac{1}{r_n}. \quad (11)$$

207 From the posterior probability densities of the sedimentation rates  $r_n$ , and hence  $\Delta z/r_n$ , we  
 208 can now calculate the uncertainties of the times. From the variances of the distributions of  
 209  $\Delta z/r_n$  for all layers  $n$ , we can obtain the variance of  $t(z_0 + N\Delta z)$  by a simple summation:

$$\text{Var}(t(z_0 + N\Delta z)) = \sum_{n=1}^N \text{Var} \left( \frac{\Delta z}{r_n} \right). \quad (12)$$



210 Working with variances, instead of the full probability distributions for the inverse sedimentation rates, saves computer storage and time when processing large data sets. Furthermore, 211 due to the central limit theorem, the distribution of the sum of random time increments 212 will converge to a Gaussian distribution when the number of layers increases, making the 213 variance an adequate description of the uncertainty. 214

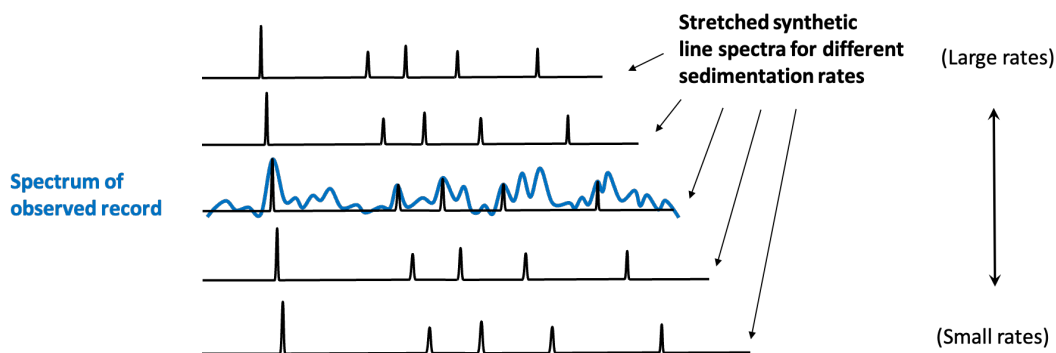


Figure 1: Schematic overview of the likelihood calculation for fitting Milankovitch cycles in elemental profiles. The spectrum of the observed geochemical signal (e.g., Al content) is compared against a theoretical line spectrum, composed of known astronomical frequencies, and stretched according to the sedimentation rate. The likelihood of each assumed sedimentation rate is computed from the probabilities that amplitudes at line locations are significant peaks. This process yields probability distributions of sedimentation rates as a function of depth, and allows an age–depth model consistent with Milankovitch forcing to be computed.

## 215 2.6 The AstroComb Algorithm

216 ASTROCOMB implements the above approach through the following steps:

- 217 1. **Preprocessing:** Detrend and normalise the depth series, optionally re-sample or 218 smooth.
- 219 2. **Sliding Window:** For each depth window (e.g., 2–4 m interval), compute the local 220 power spectrum.
- 221 3. **Spectral Inversion:** Fit the observed spectrum to the target astronomical model and 222 estimate the posterior probability distribution of the sedimentation rate.
- 223 4. **Output:** Store the sedimentation rate  $r(z)$  and its posterior probability distribution 224 for the window.

225 Every step in our calculation is accompanied by an uncertainty estimate. For each position 226 of the sliding data window, the total noise on the signal (measurement noise on the data 227 from the XRF scanner, and "geological noise" defined as signal that is not measurement 228 noise or Milankovic signal) is automatically estimated by the algorithm (see the likelihood 229 calculation above).



### 230 3 Results

231 To illustrate the application of the multichannel, probabilistic Milankovitch period detector,  
232 **AstroComb**, we analysed high-resolution XRF data from a ~20-meter long interval of the  
233 Fågeltofta-2 drill core through the Alum Shale Formation in southern Sweden. Given that  
234 the XRF measurements were collected with a sampling resolution of 0.0002 meters and  
235 captured the concentrations of at least 22 elements, incl.  $\text{Al}_2\text{O}_3$ ,  $\text{SiO}_2$ , S,  $\text{K}_2\text{O}$ , CaO,  $\text{TiO}_2$ ,  
236 V, MnO,  $\text{Fe}_2\text{O}_3$ , Ni, Cu, Zn, Ge, As, Rb, Sr, Y, Zr, Mo, Ba, Hf, and U, this extensive  
237 elemental dataset formed the basis for the spectral analysis. Figure 2 shows a subset (the  
238 top 40 mm) of the data from ~19 m of core, yielding ~90,000 measurements.

239 We simultaneously searched for 4 canonical Milankovitch periods applicable to the late  
240 Cambrian area at 494 Ma based on [Waltham \(2015\)](#), grouped as follows:

- 241 • **Precession** (in ky): 19.5
- 242 • **Obliquity** (in ky): 32.4
- 243 • **Eccentricity** (in ky): 405, 99

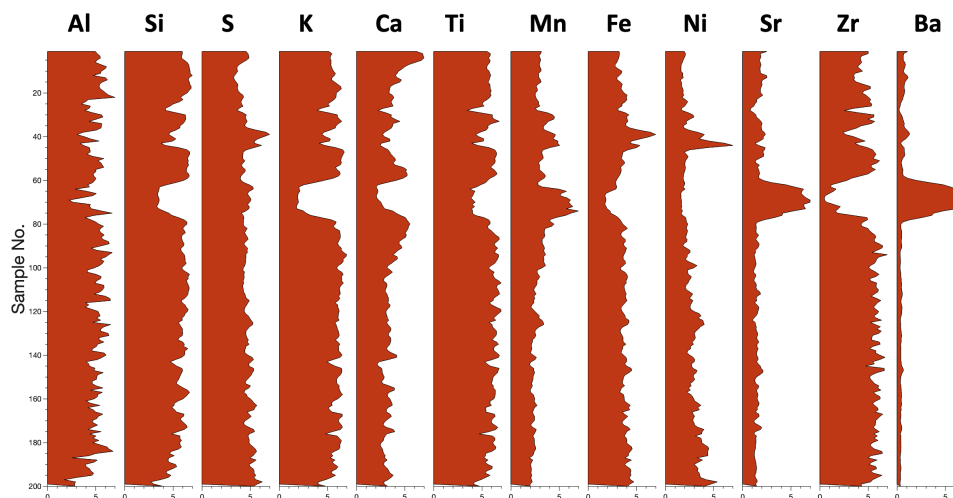


Figure 2: A selection of concentration profiles of the Fågeltofta Alum Shale core, measured via XRF core scanning at 0.2 mm resolution. The dataset spans approximately 19 meters of stratigraphy and comprises ~ 90,000 individual measurements. Several profiles show well-developed quasi-periodic oscillations, which serve as the primary proxy for detecting orbitally forced sedimentary cycles in the subsequent astrochronological analysis.

244 We selected Al as the primary input because of its robustness as a proxy for detrital  
245 input and its strong spectral structure in preliminary analysis ([Sørensen et al. \(2020\)](#); [Zhao  
246 et al. \(2022\)](#)). The depth series was detrended with a linear function. ASTROCOMB was run  
247 using a window length of 3.3 m, stepped every 0.2 mm.

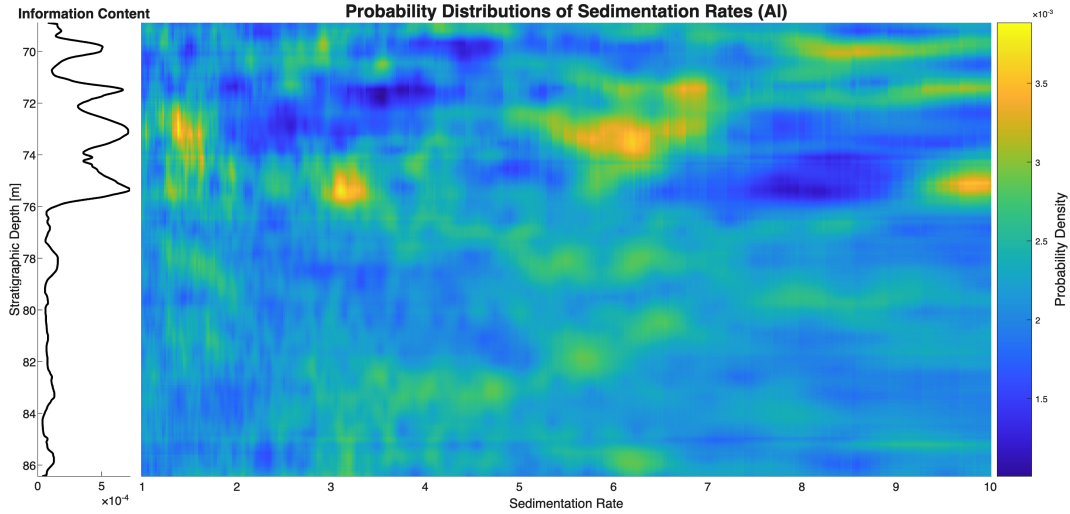


Figure 3: Sedimentation rate probability distribution for the Fågeltofta-2 core. The information content about Milankovic cycles contained in the XRF data is shown (green curve) as quantified by the Kullback-Leibler measure.

248 The bulk sedimentation rate was *a priori* found within a range of realistic sedimentation  
 249 rates from 1.0 to 10.0 mm/ky. As output, we show the a posteriori probability distribution  
 250 of the sedimentation rates versus stratigraphic depth (figure 3), and selected spectral fits  
 251 for each 2 m in the core (figure 4). Also, we introduce the Kullback-Leibler information  
 252 measure at each depth  $z$  showing how much Milankovic information is present in the data  
 253 as a function of depth. This is obtained from:

$$\mathcal{I} = \int_R P_z(r) \ln \left( \frac{P_z(r)}{U(r)} \right) dr \quad (13)$$

254 where  $P_z(r)$  is the calculated probability distribution of  $r$  at depth  $z$ ,  $R$  is the range of  
 255 sedimentation rates, and  $U(r)$  is a uniform (non-informative) distribution. Figure 3 shows  
 256 that Milankovic cycles information is present in the core, and that the sedimentation rates  
 257 vary also within information-dense intervals.

258 From the estimated sedimentation rates, a Milankovitch timescale and its uncertainty  
 259 was derived (Figure 5), using the age of 496.595 Ma, consistent with Sørensen et al. (2020),  
 260 at a stratigraphic depth of 86.005 m as a reference. This timescale enables the estimation of  
 261 relative geological ages across the core, and allows depth-indexed chemical data to be analysed  
 262 in the temporal domain, significantly enhancing our ability to interpret environmental  
 263 transitions over geological timescales.

264 To demonstrate ASTROCOMB's capability of multi-channel analysis of several basic ele-  
 265 ments records to obtain improved resolution of the Milankovic cycles, we simultaneously ran  
 266 the algorithm on the S, Al and Mn records. The result, which is given in figure 6, shows that

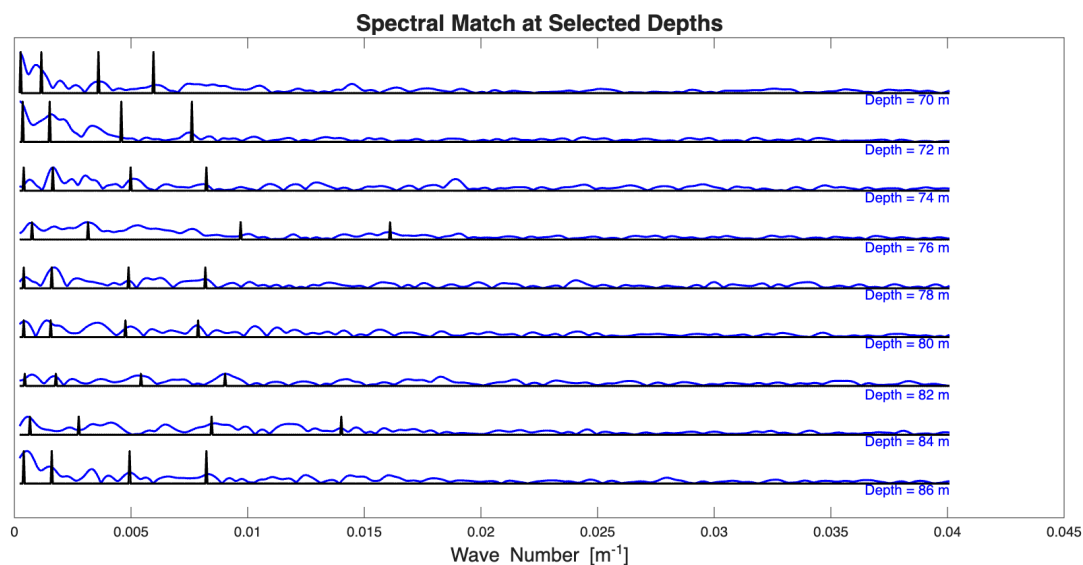


Figure 4: Spectral match at selected stratigraphic depths in the Fågeltofta-2 core. For every 2 m, the spectral lines corresponding to the best Milankovitch match are plotted together with spectra of data observed in windows centered at the depth.

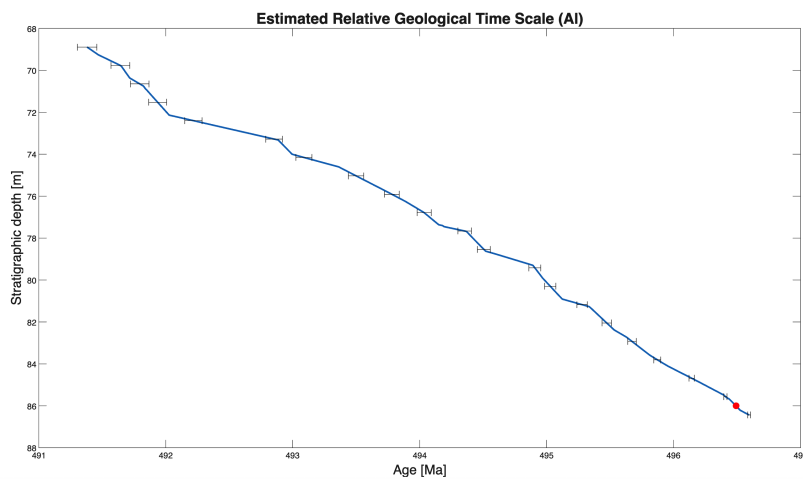


Figure 5: Estimated geological timescale and its uncertainty (standard deviations), based on probabilistic estimation of instantaneous sedimentation rates from the AI record in the Fågeltofta-2 core. The timescale is anchored at 86.005 m, corresponding to 496,595 ky (Sørensen et al. (2020)). This is marked on the graph.

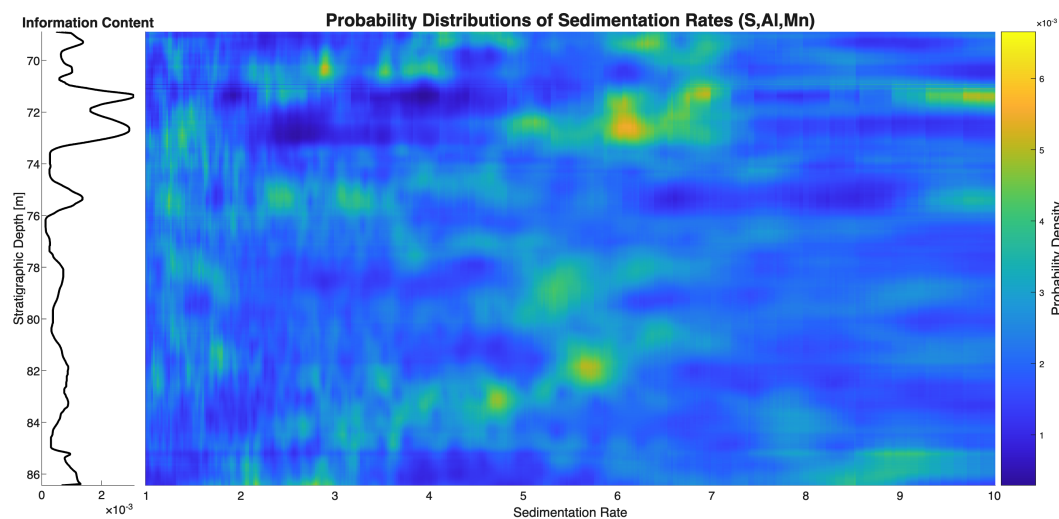


Figure 6: Probabilistic analysis of sedimentation rates in the Fågeltofta-2 core, based on simultaneous processing of S, Al, and Mn. Comparing to figure 3 it is clear that this multi-channel analysis has provided a higher resolution with more distinct peaks in the probability densities.

267 the resolution has improved, compared to the single-channel result in figure 3. High proba-  
268 bilities have increased, and low probabilities have decreased. The overall picture is generally  
269 the same, but several secondary peaks, indicating possible alternative solutions, are reduced  
270 or have disappeared. The corresponding relative time scale is shown in figure 7. The overall  
271 picture is similar to figure 5, but there is more detail, and the total time span is somewhat  
272 increased.

273 The results support the use of high-resolution XRF data coupled with probabilistic spec-  
274 tral inversion as a powerful tool for extracting geochronological information from ancient  
275 sedimentary archives.

## 276 4 Discussion

277 Extensive tests were carried out to study the accuracy and stability of the algorithm. A  
278 severe test with artificial data with 200% noise, showing significant sedimentation rate dis-  
279 continuities, was carried out. The synthetic sedimentation rate model, seen in figure 8, is  
280 characterized by layers with realistic sedimentation rates, and separated by significant dis-  
281 continuities. From this model, the synthetic data were calculated (see figure 10). The 200%  
282 noise was red noise with a  $1/f^2$  power spectral density, simulating a background spectrum  
283 of geological signal that cannot be explained as astronomical forcing. Figure 10 shows the  
284 posterior probability densities of sedimentation rates for all depths, computed by **AstroComb**  
285 using the synthetic data. The true result (the synthetic model) is overlain to show the fidelity

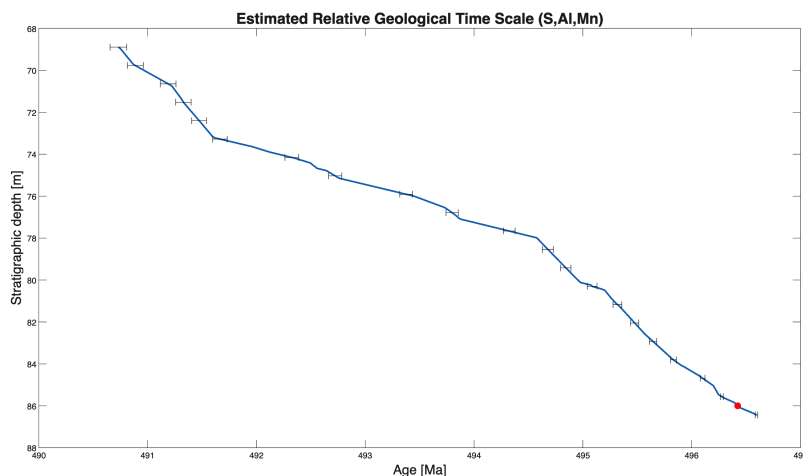


Figure 7: Relative timescale computed from the multi-channel data with records of S, Al and Mn.

286 of the reconstruction. Considering the very high noise level, the reconstruction of the true  
287 sedimentation rates is excellent. However, the test also illustrates how artifacts (possible,  
288 incorrect sedimentation rates) are introduced by the noise, the variability of the true model,  
289 and the non-linearity of the problem. Some of these spurious features could be interpreted as  
290 true sedimentation rates. This is a challenge, but, on the other hand, all true sedimentation  
291 rates are found by the algorithm, and the large discontinuities between layers of constant rates  
292 are quite well reconstructed, despite the high noise level.

293 This study demonstrates that the **AstroComb** method extends the spectral misfit min-  
294 imization strategy in a probabilistic framework, handling uncertainty propagation and pa-  
295 rameter tuning with statistical rigor.

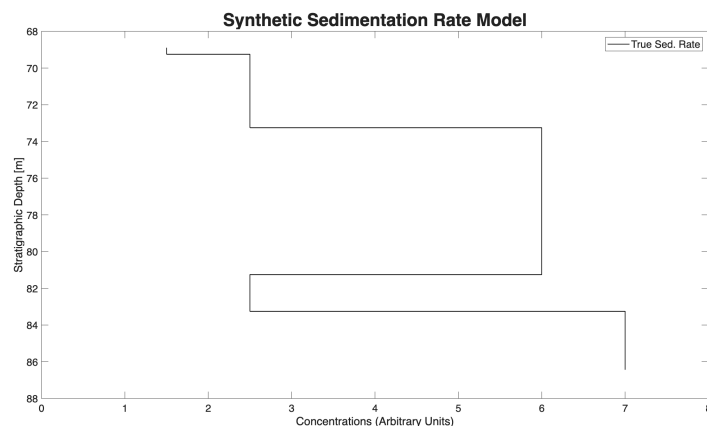


Figure 8: Synthetic sedimentation rate model used in the testing of the algorithm. The model has layers with realistic sedimentation rates, and the layers are separated by significant discontinuities.

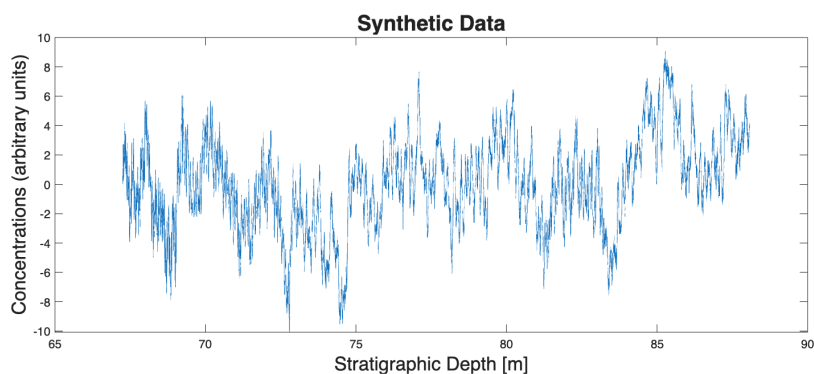


Figure 9: Synthetic data with 200% red noise used to test of the algorithm.

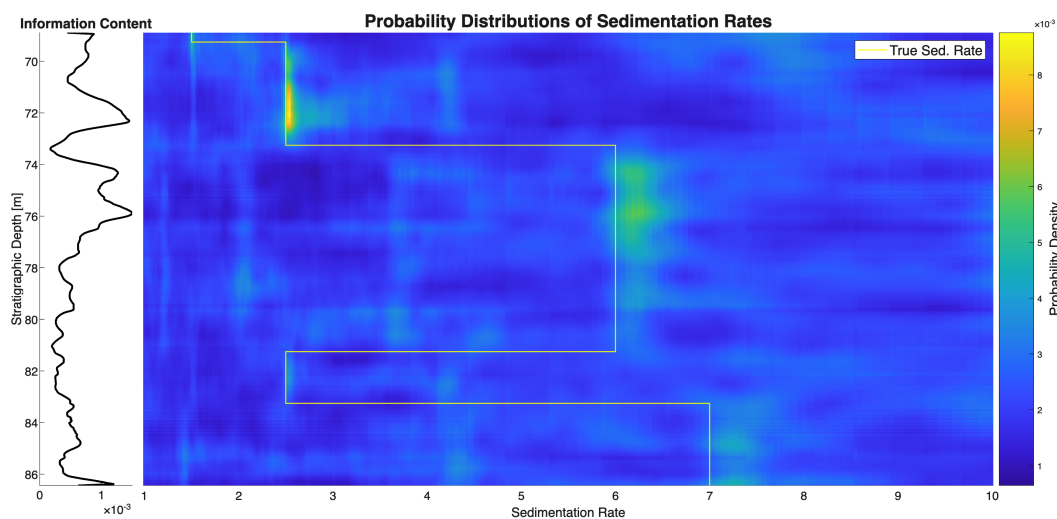


Figure 10: Probability densities of sedimentation rates, computed from the synthetic data with 200% red noise. The synthetic model is overlain to show the fidelity of the reconstruction. In view the very high noise level, the reconstruction of the true sedimentation rates is very good. However, the test also shows how artifacts are introduced by the noise, the variability of the true model, and the non-linearity of the problem.



## 296 4.1 Limitations

297 Nonetheless, some limitations must be acknowledged. The assumed orbital target periods  
298 are model-based and cannot be empirically verified for the Cambrian. While the tuning  
299 strategy relies on the 405 kyr eccentricity cycle as a stable chronometer, potential shifts in  
300 Earth's rotational parameters due to e.g. tidal dissipation effects could introduce biases.

301 Our algorithm is based on the assumption that prior information about the spectral peak  
302 identification process can be provided, and that it adequately describes the way Milankovic  
303 periods are identified by human analysts. According to our synthetic tests, and the good  
304 consistency of our Fågeltofta results with results from previous studies, it works well, but it  
305 is advisable to carefully check results obtained in new cases, particularly to what extent they  
306 are compatible with other, independent knowledge about the geological scenario considered.

307 There are also some fundamental assumptions behind Milankovic analysis that apply to  
308 any method. Milankovic cycles are (quasi-)periodic, but not sinusoidal. This means that a  
309 hypothetical, noise-free Milankovic spectrum will, in general, contain spectral components  
310 outside the main Milankovic frequencies. These components are generally disregarded in  
311 Milankovic analysis programs, including *AstroComb*. More seriously, the Earth's sedimentary  
312 system is highly nonlinear and is therefore expected to produce additional periods that are  
313 sums and differences of the main Milankovic cycles. The amplitudes of such periods could  
314 be significant, but they are ignored by our algorithm. An additional problem with the non-  
315 linearity of the sedimentary system is that, even if we know the amplitudes of the input  
316 Milankovic signal, the output amplitudes observed in boreholes are entirely unknown. This  
317 was the background for the the way that we implemented our spectral fit algorithm.

318 Last, but not least, it is important to remember that Milankovic cycle identification is a  
319 *difficult* problem. The signal-to-noise ratio is generally very low, and the problem is often  
320 similar to finding a needle in a hay stack. Such problems are prone to detrimental human  
321 biases, but *AstroComb* is designed with the aim of quantifying the analysis, and casting the  
322 problem as a probabilistic inference problem, so as to avoid such biases. It generally provides  
323 several plausible solutions for the sedimentation rates at given depths, allowing the user to  
324 choose, based on geological/stratigraphic knowledge.

## 325 4.2 Broader Implications

326 The *AstroComb* algorithm has discovered abrupt changes in sedimentation rate in the Fågeltofta  
327 core, making predictions to guide sedimentologist in reconstructing pulses of sedimentation  
328 from geological archives. As sedimentation rate is a fundamental parameter characteriz-  
329 ing a sedimentary environment and a factor that serves as a first order control on organic  
330 matter preservation, *AstroComb* may help engaging sedimentologists with a new relative  
331 chronometer. Also, we envision to use it in combination with geochemical information about  
332 sedimentation rate changes.

## 333 5 Conclusion

334 Our algorithm contributes methodologically to the field of deep-time astrochronology by  
335 offering a multi-channel, probabilistic method for estimation of astronomically constrained



336 timescales. At the same time we offer critical quality control of the data, allowing the user  
337 to evaluate how much Milankovic information can actually be detected in the basic elements  
338 records. The framework established here provides a robust platform for exploring the causes  
339 and consequences of climatic, geochemical, and evolutionary change in Earth's early history.

## 340 6 Code and Data Availability

341 The current version, which is the exact version of the program used to produce the results  
342 used in this paper, as well as the input data and scripts to run the model and produce  
343 the plots for all the simulations, is available at <https://doi.org/10.5281/zenodo.17966227>  
344 (Fernandes (2025)) under the licence GNU General Public License v3.0.

## 345 7 Author Contributions

346 Iris Fernandes and Klaus Mosegaard led the conceptualization of the study and the devel-  
347 opment of the methodology, including algorithm design, numerical analysis, inverse prob-  
348 lem formulation, and the integration of uncertainty quantification. They implemented the  
349 data processing and analysis pipeline, contributed to the overall methodological design, and  
350 drafted the original manuscript. Tais W. Dahl and Aske Sørensen contributed to the theoret-  
351 ical framework and provided critical input on the geochemical and geological interpretation  
352 and analysis. Mohammad Yousof contributed to algorithm parameterization and optimiza-  
353 tion. Nicholas Thibault contributed with geochronological insights in the analysis.

## 354 References

- 355 Dahl, T. W., Siggaard-Andersen, M.-L., Schovsbo, N. H., Persson, D. O., Husted, S.,  
356 Hougård, I. W., Dickson, A. J., Kjær, K., and Nielsen, A. T. (2019). Brief oxygenation  
357 events in locally anoxic oceans during the cambrian solves the animal breathing paradox.  
358 *Scientific Reports*, 9:11669.
- 359 Farhat, M., Auclair-Desrotour, P., Boué, G., and Laskar, J. (2022). The resonant tidal  
360 evolution of the earth–moon distance. *Astronomy Astrophysics*, 665:L1.
- 361 Fernandes, I. (2025). AstroComb-1.0.
- 362 Fernandes, I., Mosegaard, K., and Dahl, T. W. (2026). Probe4t: Geochemically informed  
363 sedimentation rate estimation in ultra-high stratigraphic resolution. Submitted to Geosci-  
364 entific Model Development.
- 365 Hays, J. D., Imbrie, J., and Shackleton, N. J. (1976). Variations in the earth's orbit: Pace-  
366 maker of the ice ages. *Science*, 194(4270):1121–1132.
- 367 Hoang, N., Laskar, J., Hara, N. C., Wu, Y., Sultanov, A., Sinnesael, M., Westerhold, T.,  
368 and Bujons, P. (2025). Astrogeofit: A genetic algorithm and bayesian approach for the as-



- 369      tronomical calibration of the geological timescale. *Paleoceanography and Paleoclimatology*,  
370      40(8):e2024PA005021.
- 371      Kemp, D. B. and Sexton, P. F. (2014). Time-scale uncertainty of abrupt events in the  
372      geologic record arising from unsteady sedimentation. *Geology*, 42(10):891–894.
- 373      Laskar, J., Fienga, A., Gastineau, M., and Manche, H. (2011). A new orbital solution for  
374      the long-term motion of the earth. *Astronomy Astrophysics*, 532:A89.
- 375      Laskar, J., Robutel, P., Joutel, F., Gastineau, M., Corrêa, A. C. M., and Levrard, B. (2004).  
376      A long-term numerical solution for the insolation quantities of the earth. *Astronomy*  
377      *Astrophysics*, 428(1):261–285.
- 378      Li, M., Kump, L. R., Hinnov, L. A., and Mann, M. E. (2018). Tracking variable sedi-  
379      mentation rates and astronomical forcing in phanerozoic paleoclimate proxy series with  
380      evolutionary correlation coefficients and hypothesis testing. *Earth and Planetary Science*  
381      *Letters*, 501:165–179.
- 382      Meyers, S. R. (2015). The evaluation of eccentricity-related amplitude modulation and  
383      bundling in paleoclimate data: An inverse approach for astrochronologic testing and  
384      timescale optimization. *Paleoceanography*, 30(12):1625–1640.
- 385      Meyers, S. R. (2019). Cyclostratigraphy and the problem of astrochronologic testing. *Earth-*  
386      *Science Reviews*, 190:190–223.
- 387      Meyers, S. R. and Malinverno, A. (2018). Proterozoic milankovitch cycles and the history of  
388      the solar system. *Proceedings of the National Academy of Sciences*, 115(25):1717689115.
- 389      Meyers, S. R., Sageman, B. B., and Hinnov, L. A. (2001). Integrated quantitative stratigra-  
390      phy of the cenomanian-turonian bridge creek limestone member using evolutive harmonic  
391      analysis and stratigraphic modeling. *Journal of Sedimentary Research*, 71(4):628–644.
- 392      Meyers, S. R., Sageman, B. B., and Hinnov, L. A. (2008). Resolving milankovitch: Consid-  
393      eration of signal and noise. *Paleoceanography*, 23(2):PA2202.
- 394      Nielsen, A. T., Schovsbo, N. H., Klitten, K., Woollhead, D., and Rasmussen, C. (2018).  
395      Gamma-ray log correlation and stratigraphic architecture of the cambro-ordovician alum  
396      shale formation on bornholm, denmark: evidence for differential syndepositional isostasy.  
397      *Bulletin of the Geological Society of Denmark*, 66:237–273.
- 398      Sørensen, A. L., Nielsen, A. T., Thibault, N., Zhao, Z., Schovsbo, N. H., and Dahl, T. W.  
399      (2020). Astronomically forced climate change in the late cambrian. *Earth and Planetary*  
400      *Science Letters*, 548:116475.
- 401      Waltham, D. (2015). Milankovitch period uncertainties and their impact on cyclostratigra-  
402      phy. *Journal of Sedimentary Research*, 85:990–998.
- 403      Weedon, G. P. (2003). *Time-Series Analysis and Cyclostratigraphy: Examining Stratigraphic*  
404      *Records of Environmental Cycles*. Cambridge University Press, Cambridge, UK.



405 Zhao, Z., Thibault, N. R., Dahl, T. W., Schovsbo, N. H., Sørensen, A. L., Rasmussen, C.  
406 M. , and Nielsen, A. T. (2022). Synchronizing rock clocks in the late cambrian. *Nature*  
407 *Communications*, 13:1990.